01 May 2013, 4:30 pm - 5:15 pm

# Performance Appraisal of Ballasted Rail Track Stabilised by Geosynthetic Reinforcement and Shock Mats

Buddhima Indraratna
*University of Wollongong, Australia*

Sanjay Nimbalkar
*University of Wollongong, Australia*

Cholachat Rujikiatkamjorn
*University of Wollongong, Australia*

Commemorate the Legacy of Ralph B. Peck
April 29 - May 4, 2013 CHICAGO
Seventh International Conference on
Case Histories in Geotechnical Engineering
and Symposium in Honor of Clyde Baker

# PERFORMANCE APPRAISAL OF BALLASTED RAIL TRACK STABILISED BY GEOSYNTHETIC REINFORCEMENT AND SHOCK MATS

**Buddhima Indraratna**
Professor of Civil Engineering, and Research Director
Centre for Geomechanics and Railway Engineering,
University of Wollongong
NSW 2522 AUSTRALIA

**Sanjay Nimbalkar**
Research Fellow
Centre for Geomechanics and Railway Engineering,
University of Wollongong
NSW 2522 AUSTRALIA

**Cholachat Rujikiatkamjorn**
Senior Lecturer
Centre for Geomechanics and Railway Engineering,
University of Wollongong
NSW 2522 AUSTRALIA

ABSTRACT

Rail tracks serve the principal mode of transportation for bulk freight and passengers in Australia. Ballast is an essential constituent governing the overall stability and performance of rail tracks. However, large repetitive loads from heavy haul and passenger trains often lead to excessive deformation and degradation of the ballast layer, which necessitate frequent and expensive track maintenance works. In Australia, the high cost of track maintenance is often associated with ballast degradation, fouling (e.g. coal and subgrade soil) and associated poor drainage, differential settlement of track, pumping of subgrade soils, and track misalignment due to excessive lateral movements. With increased train speeds, the track capacity is often found to be inadequate unless more resilient tracks are designed to withstand the substantially increased vibration and repeated loads. A field trial was conducted on a section of track in Bulli, New South Wales, and findings indicated that the moderately-graded recycled ballast when used with a geocomposite resulted in smaller deformations in both vertical and lateral directions in comparison to uniformly-graded fresh ballast. Installing resilient (shock) mats in the track substructure led to significant attenuation of high impact forces and thereby mitigated ballast degradation. In addition, a series of full-scale field experiment was undertaken on track sections near Singleton, New South Wales to investigate the effects of geosynthetics on the performance of the track built on subgrade soils with varying stiffness. The finding suggested that geogrids can decrease vertical strains of the ballast layer and a few selected types of geogrids can be used more effectively with soft subgrade soils. This state of the art & practice (SOAP) paper describes the results of two unique full-scale field trials, series of large-scale laboratory tests and numerical models to assess the improved performance of ballasted rail tracks using synthetic grids and shock mats.

## INTRODUCTION

Frequent traffic congestion on roads and the demand for quicker and safer transport have made the railways the most demanded means of public transportation in many countries. Among railroad structures, ballasted track is the most popular due to its relatively lower cost of construction. A typical ballasted track is composed of graded layers of rock fragments placed below the rail-sleeper assembly. The ballast layer should provide the optimum resiliency, thereby transmitting the imposed wheel loading to an acceptable depth of the subgrade soils while preventing excessive settlement and lateral spread. The granular nature of ballast should also ensure efficient drainage of the track, so that no pore water pressures are allowed to develop. In recent times, ballast degradation and track deformation is clearly associated with increased cyclic and impact loads, leading to significantly high maintenance costs. In many countries including North America, a large proportion of the maintenance budget is usually spent on ballast replacement and related activities (Chrismer 1985). In Australia, over 30 millions of dollars is spent annually on track maintenance. For example, in NSW

alone, approximately 1.3 million tonnes of ballast was consumed at a cost of over 12 million dollars (Indraratna *et al*. 2011c). Unless the proper role of geotechnical parameters which control the ballast stress-strain behaviour under static and repeated loads is carefully examined, the cost of track maintenance will continue to rise. The breakage of asperities and crushing of rock aggregates under high cyclic and impact loading, causes differential track settlement that adversely affects track geometry and results in more frequent maintenance (Marshal 1973, Indraratna *et al*. 2005, Hossain *et al*. 2007, Lackenby *et al*. 2007).

The potential use of geosynthetics to improve track stability has been observed in several laboratory studies (Selig and Waters 1994, Raymond 2002, Shin *et al*. 2002, Indraratna and Salim 2003, Indraratna *et al*. 2006, 2007, Indraratna and Nimbalkar 2012). The laboratory studies by Brown *et al*. (2007) and Indraratna *et al*. (2011b) have shown that the effectiveness of geogrid reinforcement is highly dependent on the stiffness and size of the apertures. A 30% increase in the stiffness of geogrid has resulted in up to 20% smaller vertical strain on the ballast, while the apertures providing the best interlocking between the geogrids and ballast are between 1.1 and 1.7 times the median particle size ($d_{50}$) of the ballast.

The infiltration of fouling material decreases the void ratio and restricts track drainage. The crushed rock fines (due to particle breakage), coal fines (due to spillage from coal wagons) and clay-silt fines (due to pumping of soft saturated subgrade) accumulate within the voids (i.e. fouling) of the ballast bed and impede track drainage. The magnitude of the impact loads vary depending upon irregularities in the wheels or rails, and the dynamic response of the track (Jenkins *et al*. 1974, Auersch 2006, Indraratna *et al*. 2011b). Installing resilient mats such as rubber pads (shock mats) in rail tracks can substantially attenuate the dynamic impact force (Nimbalkar *et al*. 2012). Field studies in combination with laboratory tests often represent an efficient strategy for accurately assessing rail track degradation due to impact loads. Extensive field trials on sections of instrumented railway track at Bulli and Singleton, New South Wales (NSW), Australia have been conducted. This paper describes the results the two unique full-scale field trials and series of large-scale laboratory tests and numerical modelling using Finite Element Method (FEM) and Discrete Element Method (DEM) to assess the performance of ballasted rail tracks using synthetic grids and shock mats.

## GEOTECHNICAL BEHAVIOUR OF BALLAST

Ballast is usually composed of blasted (quarried) rock aggregates originating from high quality igneous or metamorphic rock quarries and usually includes dolomite, rheolite, gneiss, basalt, granite, and quartzite (Raymond 1979). It is composed of medium to coarse gravel sized aggregates (10 - 60 mm). Ballast should possess angular particles of high specific gravity, high shear strength, high toughness and hardness, high resistance to weathering, and a minimum of hairline cracks (Indraratna *et al*. 2011c).

### Shear Strength

The Mohr-Coulomb theory is conveniently used to describe the shear behaviour of ballast. The non-linear strength envelope is markedly curved as shown in Fig. 1. The non-linearity is pronounced at smaller confining pressures. The non-linear strength envelope is associated with the dilatant behaviour of rock fragments at low normal stress. Normal stresses below 400 kPa are usually representative of typical ballasted tracks (Jeffs and Tew 1991). The variation of apparent friction angle ($\phi_p'$) corresponding to the peak deviator stress is also plotted in Fig. 1. In railway ballast, where the confining pressure is low, the apparent friction angle is expected to be relatively high ($\phi_p' > 40°$). The same material at relatively high confining pressure will indicate a reduced friction angle in the order of 35°.

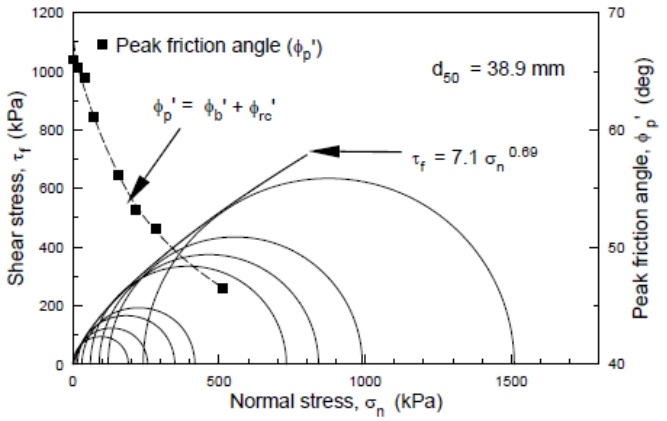


*Fig. 1. Mohr-Coulomb failure envelopes for Latite Basalt (data sourced from Indraratna et al, 1998).*

### Ballast Breakage

The ballast degradation is a complex mechanism that usually initiates with the breakage of asperities (sharp corners/projections), followed by complete crushing of weaker particles under further loading. Indraratna *et al*. (2005) introduced a new Ballast Breakage Index (BBI) specifically for railway ballast to quantify the extent of degradation, and it is based on the particle size distribution (PSD) curves. The ballast breakage index (BBI) is calculated on the basis of changes in the fraction passing a range of sieves, as shown in Fig. 2. The increase in extent of particle breakage causes the PSD curve to shift further towards the smaller particles size region on a conventional PSD plot. An increase in the area A between the initial and final PSD results in a greater BBI value. BBI has a lower limit of 0 and an upper limit of 1. By referring to the linear particle size axis, BBI can be calculated by using following equation.

$$BBI = \frac{A}{A + B} \quad (1)$$

where A is the area defined previously, and B is the potential breakage or area between the arbitrary boundary of maximum breakage and the final particle size distribution.

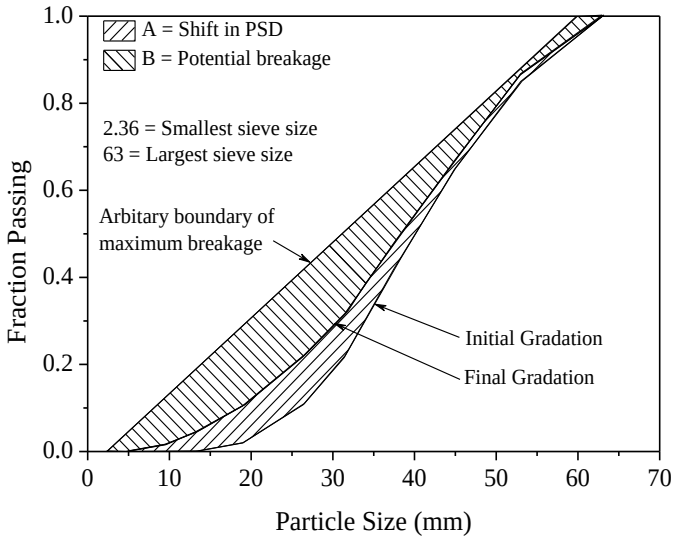


*Fig. 2. Ballast breakage index (BBI) calculation method (data sourced from Indraratna et al. 2005).*

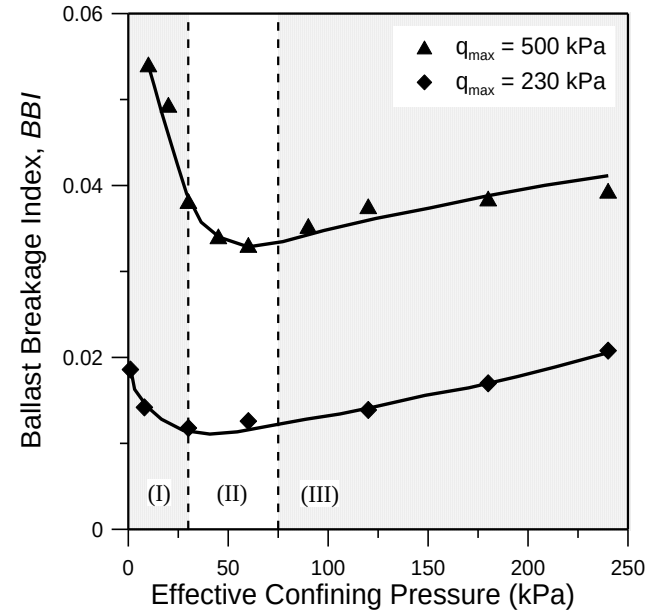


*Fig. 3. Effect of confining pressure on particle degradation (data sourced from Indraratna et al. 2005).*

Effect of Confining Pressure

Indraratna *et al*. (2005) proposed that the degradation of ballast under cyclic loading can be categorised into three distinct zones, namely: (I) the Dilatant Unstable Degradation Zone (DUDZ: $\sigma_3' < 30$ kPa), (II) the Optimum Degradation Zone (ODZ: $\sigma_3' = 30$ - 75 kPa), and (III) the Compressive Stable Degradation Zone (CSDZ: $\sigma_3' > 75$ kPa), as shown in Fig. 3.

In the DUDZ zone, specimens are characterised by limited particle-to-particle contact areas and undergo considerable degradation as a result of shearing and attrition of angular projections. In the ODZ region, the particles are held together with enough lateral confinement to provide increased inter-particle contact areas, which in turn reduces the risk of breakage. At higher $\sigma_3'$ (CSDZ region), the particles are forced against each other, which limits any sliding or rolling, and therefore breakage is significantly increased. Due to the large lateral forces being applied to the samples in this region, volumetric compression is enhanced, which is partly due to an increase in particle breakage.

## EFFECTS OF BALLAST FOULING ON TRACK DRAINAGE AND STABILITY

Track substructure should be designed and constructed so as to drain the water into nearby drainage ditches or pipes, but fouling of ballast due to intrusion of fine material either from surface or subgrade slowly decreases its drainage capacity. In the case of poor drainage, problems may occur in the track such as (i) reduced ballast shear strength, stiffness, and load bearing capacity, (ii) increased track settlement, (iii) softening of subgrade, (iv) formation of slurry and clay pumping under cyclic loading, (v) ballast attrition by jetting action and freezing of water, and (vi) sleeper degradation by water jetting. All these problems will degrade the performance of the track and demand additional maintenance. Ballast fouling due to coal and subgrade fines, and the subsequent formation of mud holes in Goonyella System (Queensland) is shown in Figs. 4 and 5.

*Fig. 4. Mudholes caused by excessive coal/clay fouling (Photo courtesy of Michael Martin, QR National)*

*Fig. 5. Ballast fouling due to coal and subgrade pumping (Photo courtesy of Michael Martin, QR National)*

Ballast Fouling Assessment

Several fouling indices are used in practice to measure fouling. Selig and Waters (1994) have defined the fouling index as a summation of percentage (by weight) passing the 4.75mm sieve and 0.075mm sieve. They also proposed a percentage of fouling which is the ratio of the dry weight of fouled material passing through a 9.5mm sieve to the dry weight of the total fouled ballast sample. These mass based indices represent a false measurement of fouling when the fouling material has a different specific gravity. Therefore, Feldman and Nissen (2002) defined the Percentage Void Contamination (PVC) as the ratio of bulk volume of fouling material to the volume of voids of the clean ballast. However, PVC does not consider the effects of the void ratio, gradation and specific gravity of the fouling material, which is the main factor affecting ballast drainage. Therefore, a new parameter Void Contaminant Index (VCI) has been proposed to incorporate effects of void ratio, specific gravity and gradation of fouling material and ballast (Indraratna *et al*. 2010b):

$$VCI = \frac{(1+e_f)}{e_b} \times \frac{G_{sb}}{G_{sf}} \times \frac{M_f}{M_b} \times 100 \qquad (2)$$

where $e_b$ is the void ratio of clean ballast, $e_f$ is the void ratio of fouling material, $G_{sb}$ is the specific gravity of the ballast material, $G_{sf}$ is the specific gravity of the fouling material, $M_b$ is the dry mass of clean ballast, and $M_f$ is the dry mass of the fouling material. For example, a value of VCI = 100% indicates that total voids in the ballast are occupied by the fouling material. More details of VCI including field determination procedures are available in Tennakoon et al. (2012) and Indraratna et al. (2012a).

Effects of Fouling on the Track Drainage

Laboratory Testing. To study the effects of fouling, a series of large scale constant head permeability tests (AS 1289.6.7.3, 1999) on fouled ballast with different percentages of coal, clayey sand, and kaolin were conducted. The large scale permeability test chamber could accommodate specimens 500 mm in diameter and 500 mm high (Fig. 6). The fouled specimen was saturated for at least 24 hours before testing. A constant head was ensured with a steady state flow subjected to a 1.5m head of water by an adjustable overhead tank.

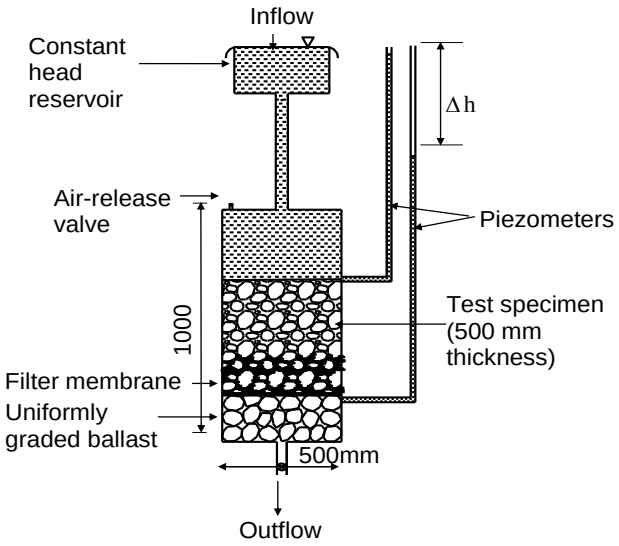


*Fig. 6. Schematic diagram of large scale permeability test apparatus*

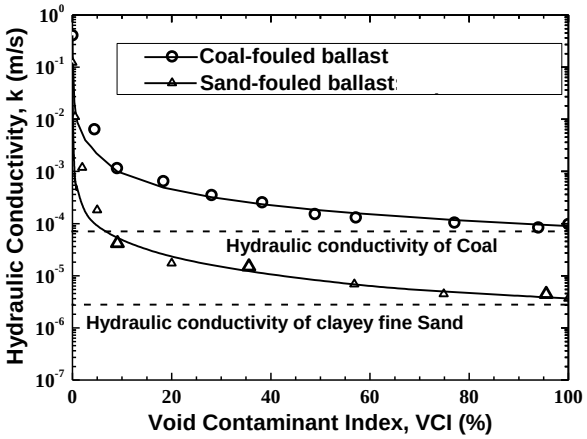


*Fig. 7. Variation of the hydraulic conductivity with VCI (data sourced from Tennakoon et al. 2012)*

Figure 7 shows the variations of hydraulic conductivity of coal fouled and sand fouled ballast with VCI where the fouling material was distributed non-uniformly. As expected, the overall hydraulic conductivity of fouled ballast always decreased with an increase in VCI. The current test results showed that a 5% increase in the VCI decreased the hydraulic conductivity by a factor of at least 200 and 1500 for ballast

contaminated by coal and clayey sand, respectively. However, this reduction in permeability would not significantly affect the minimum drainage capacity needed for acceptable track operations. Beyond a VCI of 75%, any further reduction in hydraulic conductivity becomes marginal because it approaches the hydraulic conductivity of the fouling material itself.

Two-dimensional Seepage Model. As flow through a ballasted track could occur in both vertical and horizontal directions, a two-dimensional seepage analysis was conducted using the finite element software, SEEP-W (GeoStudio, 2007), to determine the drainage capacity with respect to various fouling conditions. Hydraulic conductivity values corresponding to different VCI obtained from experimental results were used as input parameters in the analysis. The hydraulic conductivity of coarse granular materials is often dictated by the lower particle fraction size for which 15% by mass is finer (Hirschfeld 1973). The difference in values of $k_h$ and $k_v$ for coarse aggregates is considerably less than those for fine grained materials such as silt and clay. The pore structure for coarse granular materials along the vertical or horizontal directions is assumed as fairly uniform and therefore in this study $k_v$ and $k_h$ are often assumed to be same. The vertical cross section of a typical track is shown in Fig. 8a and due to symmetry, a finite element discretization of one-half track is considered in Fig. 8b.

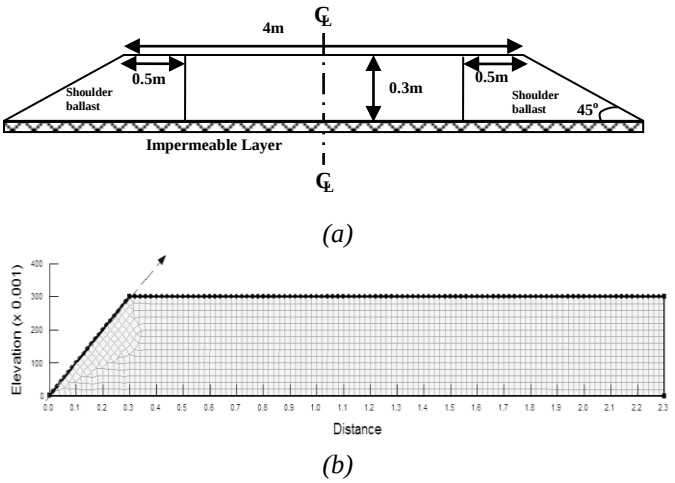


*(a)*

*(b)*

*Fig. 8. (a) Vertical cross section of the typical ballast layer used in seepage analysis and (b) Discretization of one-half track*

Three types of boundary conditions were applied to the finite element model. While a free drainage boundary condition was used at the top of the shoulder ballast surface, along the centreline, and at the bottom of the ballast bed, an impermeable boundary was applied at the bottom of the ballast bed. A hydraulic head equal to the track height was assumed at the top surface for calculating the steady state discharge ($q$). Erosion of fouled materials is neglected in this simplified model. Three possible scenarios for track fouling were simulated as described below:

Newly constructed track: The entire load bearing ballast is divided into three equal horizontal layers and the hydraulic conductivity values corresponding to different VCI values are employed.

Fouled track subjected to undercutting: The ballast is divided into two horizontal layers and the bottom ballast layer is characterised by VCI of 100%, while the top layer contains clean ballast. The thickness of clean ballast layer is varied to determine the minimum depth of clean ballast to satisfy acceptable drainage.

Track subjected to shoulder cleaning: The whole track is divided into 4 parts, shoulder ballast and 3 horizontal ballast layers with different values of VCI.

Classification of Track Drainage. The rainfall in Australia usually varies from 125 mm/hr to 175 mm/hr (Pilgrim 1997, ARTC 2006). A maximum rainfall intensity of 150 mm/hr was adopted and this would correspond to a critical flow rate ($Q_c$) of 0.0002 $m^3/s$ over the unit length of the track (Tennakoon et al. 2012).

From the seepage analysis, the maximum drainage capacity (Q) of the ballast layer can be determined for various levels and conditions of fouling. When track drainage capacity is equal to or lower than what is required for a given rainfall rate, then the fouled track is considered to be impermeable. In this context, a ratio between the computed track drainage capacity and the critical flow ($Q/Q_c$) is introduced as a dimensionless index to classify the drainage condition as stipulated in Table 1. If the ratio $Q/Q_c$ equals 1, track becomes saturated under the given rainfall. When the ratio $Q/Q_c$ is greater than 1, the track drainage is classified into various categories i.e. “Acceptable drainage”, “Good drainage”, as well as “Free drainage” and when it becomes less than 1, the drainage is classified as “Poor drainage”, “Very poor drainage”, and “Impervious” based on the output of the numerical SEEP/W analysis. It is pertinent to know that the permeability values employed in the SEEP/W analysis were chosen in accordance with the drainage criteria specified by Terzaghi and Peck (1967).

Table 1. Drainage capacity criteria

| Drainage classification | Range |
|---|---|
| Free Drainage | $Q/Q_c>100$ |
| Good drainage | $10<Q/Q_c<100$ |
| Acceptable drainage | $1<Q/Q_c<10$ |
| Poor Drainage | $0.1<Q/Q_c<1$ |
| very Poor | $0.001<Q/Q_c<0.1$ |
| Impervious | $Q/Q_c<0.001$ |

Seepage Date Interpretation. Fig. 9 shows a typical output of numerical analysis. The rainwater percolating from the top boundary moves laterally outward due to the presence of impermeable boundary at the bottom. A shift in the direction of flow at the interface between clean and fully fouled ballast (VCI = 100%) induces greater travel path and thus inhibit rapid dissipation of water.

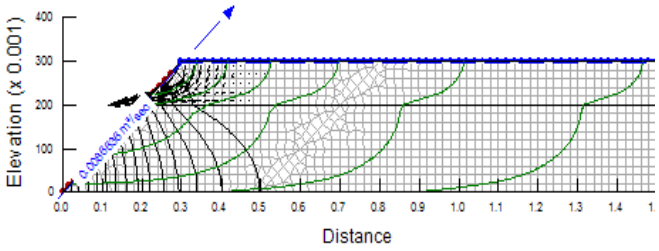


*Fig. 9. Typical output of Seepage analysis (Fouled track subjected to undercutting)*

Effects of Fouling on the Track Stability

In order to understand the effect of clay fouling on the stress-strain and degradation behaviour of ballast, for different levels of fouling (VCI = 0% to 80%), a series of large scale monotonic triaxial tests were carried out for confining pressure in the range of 10-60 kPa. Owing to the larger physical dimensions of ballast, a large-scale triaxial apparatus that could accommodate a specimen of 600 mm in height and 300 mm in diameter was used (Fig. 10).

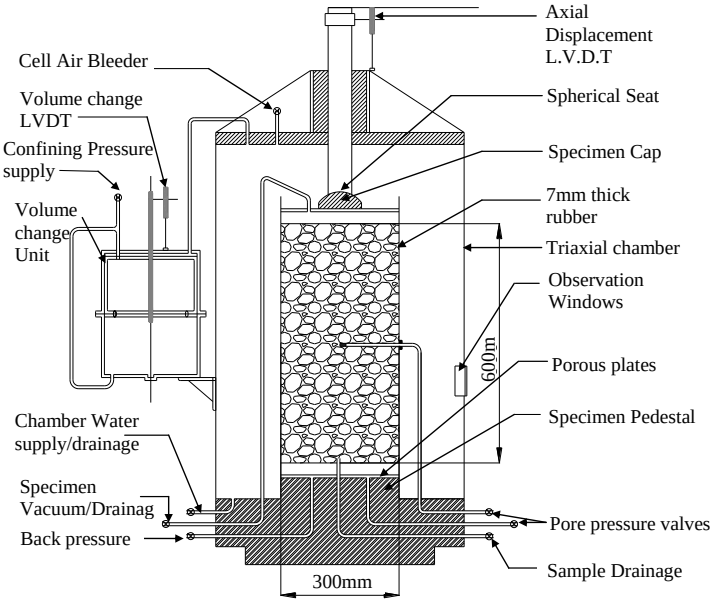


*Fig. 10. Schematic illustration of large-scale triaxial chamber (modified after Indraratna et al. 1998)*

A 7 mm thick cylindrical rubber membrane was used to prepare and confine the specimen. The Young's modulus of the membrane was determined to be 4300 kPa following the method described by ASTM D4767-02 and Bishop and Henkel (1962). The initial particle size distribution (*PSD)*, density and void ratio of ballast were kept almost identical in all specimens and were selected in accordance with the recommended Australian Standards (AS 2758.7, 1996) to capture realistic track conditions. As discussed in earlier studies, the sample size ratio (i.e. diameter of the test specimen to the maximum particle size) exceeds 6, the sample size effects become increasingly insignificant (Marachi *et al.* 1972, Indraratna *et al.* 1993). Two specimen preparation methods were adopted for different levels of *VCI* as described below:

Method 1: Preparation of clean ballast specimens. The clean ballast specimen was divided into four equal portions. Each portion was then placed inside the chamber and compacted using a vibrating plate to a height of 150 mm. All layers were placed and compacted until the final height of 600 mm was attained. The specimen was then saturated.

Method 2: Clay fouled ballast with 10%≤VCI≤80%. The amount of clay needed for predetermined VCI was calculated for each test specimen. Then a quarter of the clay was mixed with a quarter portion of ballast using the concrete mixer, and then placed inside the cylindrical membrane. A vibrating plate was used to compact the specimen following the sequential procedure as explained earlier for the subsequent layers.

After preparing the test specimen, the outer cell chamber was placed and connected to the axial loading actuator. For all the tests, back pressure of 80 kPa was applied to obtain sample saturation with Skempton's B value approaching unity (B > 0.98). During testing, the required membrane correction was carried out (ASTM D4767-02). Sieve analysis was carried out to measure BBI after each test.

Stress-strain behaviour. Figs. 11(a) and (b) illustrate the stress-strain behaviour of fouled ballast (VCI = 10 & 80%) in contrast to fresh ballast (VCI = 0%) at increasing confining pressure. As expected when VCI increases, the peak deviator stress decreases significantly. Significant clay fouling (VCI = 80%) shows an increasingly more ductile post-peak response. Figs. 11(c) and (d) show the volumetric strain changes with the axial strain for varying levels of fouling and increasing confining pressure. In the compression zone, the increasing VCI generally shows a reduced compression of the fouled specimen as the voids between the ballast grains are occupied by clay acting as void filler.

Nevertheless, in the case of VCI = 10%, an exception is observed for all three specimens (at $\sigma'_3$ = 10, 30, 60 kPa) indicating a slightly increased compression compared to their fresh ballast counterparts. This may be attributed to the small amount of clay that is coating the ballast grains as a lubricant, thereby facilitating the specimens to attain a slightly higher

compression. With respect to dilation, the highly fouled specimens show a decrease in the rate and magnitude of dilation at axial strains exceeding @ 20%, while the increase in $\sigma'_3$ from 10 to 60 kPa significantly suppresses dilation of all specimens. The addition of kaolin in sufficient quantities appears to contribute to a 'binding' effect that diminishes the tendency of the aggregates to dilate. Moreover, the specimens that are highly fouled (VCI = 80%) begin to dilate swiftly at a lower axial strain after showing a reduced compression initially compared to clean ballast. Table 2 presents the peak deviator stress with VCI.

Table 2. Variation of peak deviator stress ($q_{peak,f}$) with VCI

| VCI (%) | peak deviator stress $q_{peak,f}$ (kPa) at confining pressures $\sigma'_3$ (kPa) | | |
|---|---|---|---|
| | 10 | 30 | 60 |
| 0 | 280 | 340 | 470 |
| 10 | 225 | 290 | 415 |
| 80 | 150 | 245 | 334 |

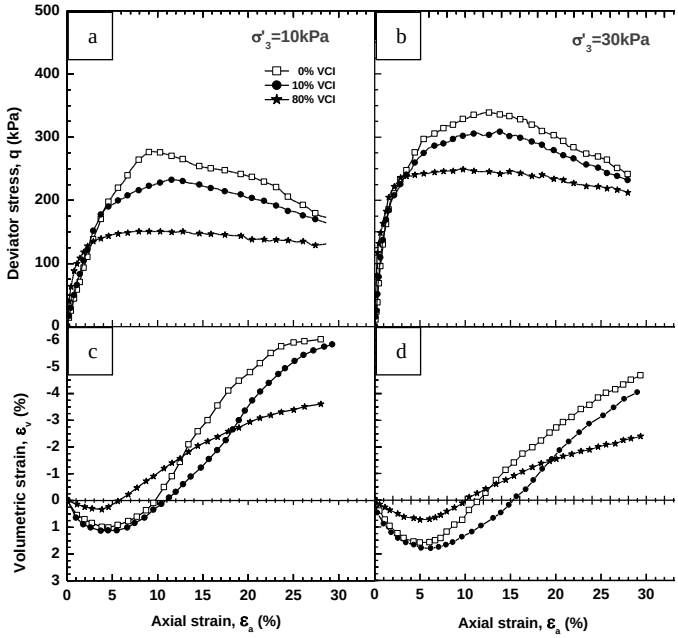


*Fig. 11. Stress-strain behaviour of clean and fouled ballast during isotropically consolidated drained tests at confining pressures ($\sigma'_3$) of (a) 10kPa, (b) 30kPa and (c) 60kPa, respectively*

The following relationship that represents the normalized shear strength of clay fouled ballast may be used in the preliminary assessment of track conditions in view of track maintenance:

$$\frac{q_{peak,f}}{q_{peak,b}} = \frac{1}{1+\beta\sqrt{(VCI)}} \quad (3)$$

where, $q_{peak,b}$ and $q_{peak,f}$ are peak deviator stresses for fresh and fouled ballast respectively; $\beta$ is an empirical parameter.

Shear Strength Envelope. The clay fouled ballast specimens exhibit a non-linear shear strength envelope similar to other rockfills (Indraratna *et al*. 1993; 1998). A non-linear shear strength envelope for clay fouled ballast can be presented in a non-dimensional form.

$$\frac{\tau_f}{\sigma_c} = m\left(\frac{\sigma'_n}{\sigma_c}\right)^n \quad (4)$$

where, $\tau$ , $\sigma'_n$ and $\sigma_c$ are shear stress, effective normal stress and uniaxial compressive strength of the parent rock (130 MPa). The empirical coefficients m and n in Eqn. (4) vary with VCI, and they are expressed as:

$$m = 0.07[1 + tanh(VCI/21.5)] \quad (5)$$

$$n = 0.56[1 + 0.3tanh(VCI/21.5)] \quad (6)$$

Assessment of Fouled Ballast using DEM Approach

The shear strength and apparent angle of the shearing resistance of clean ballast and coal fouled ballast was evaluated under various degrees of fouling using the large scale direct shear apparatus (Indraratna *et al*. 2011a). Coal fines were used as fouling material and The degree of fouling was defined by the Void Contaminant Index (VCI) defined in previous section.

This section presents the three-dimensional discrete element method (DEM) that was employed in Particle Flow Code ($PFC^{3D}$) to study the shear behaviour of fresh and coal fouled ballast in direct shear testing. 'Clump logic' in $PFC^{3D}$ was incorporated in a MATLAB code to simulate irregular shaped particles in which various groups of spherical balls were clumped together in appropriate sizes to simulate ballast particles.

A large scale shear box 300 mm long × 300 mm wide × 200 mm high, and separated horizontally into two equal boxes, was simulated with rigid walls. A free loading plate that allowed the particles to be displaced vertically during shearing was placed on the top boundary. This plate was used to apply a normal load and monitor normal displacement during shearing. The DEM simulation of this direct shear box for both fresh and fouled ballast (VCI = 40%), is shown in Fig. 12. Fouled ballast with VCI ranging from 20% to 70% were modeled by injecting a specified number of miniature spherical particles into the voids of fresh ballast.

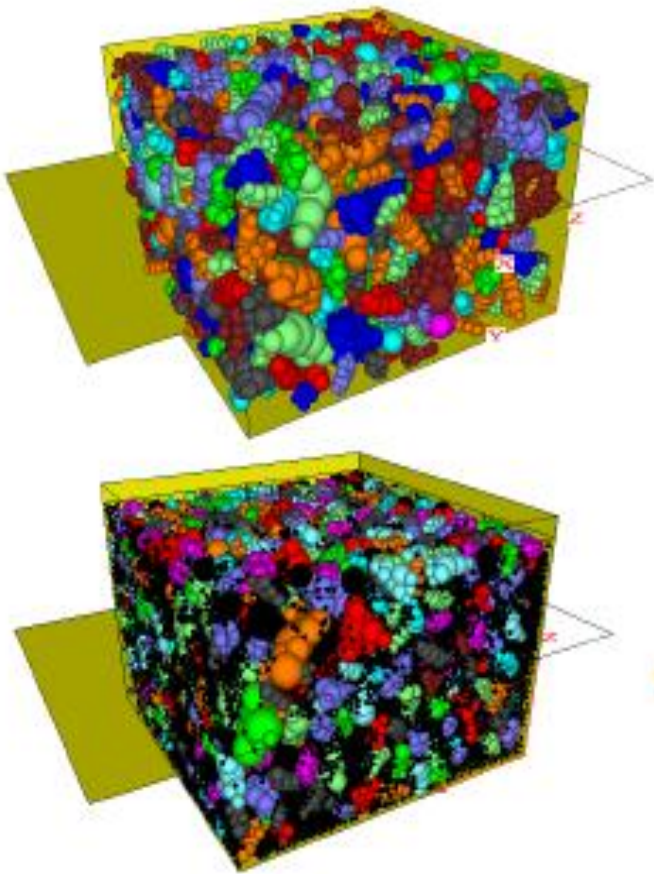

*Fig. 12. Initial assembly of large-scale direct shear test with irregular shaped particles, (a) fresh ballast and (b) 40%VCI fouled ballast (Indraratna et al. 2012b)*

The lower section of the shear box was moved at a rate of 2.5 mm/min, while the upper section of the box remained stationary. Each specimen was subjected to 37 mm of maximum horizontal displacement. During shearing, the displacement of the top plate was recorded to determine the associated volumetric deformations and a sub-routine was developed to capture the resultant forces generated at the walls in the upper section of the shear box.

DEM simulations were conducted to model fresh ballast subjected to three different normal stresses of 27kPa, 51kPa, and 75kPa. The shear stress and volumetric changes were monitored during shearing. Figure 13 shows the plots of shear stress, shear strain, and volumetric strain obtained by DEM, compared to the laboratory data reported earlier by Indraratna *et al*. (2011a). The predicted results agreed with the laboratory test findings. The post peak behaviour of ballast is similar to other rockfill aggregates of comparable sizes (e.g. Marsal 1973, Indraratna *et al*. 1998, Charles and Watts 1980).

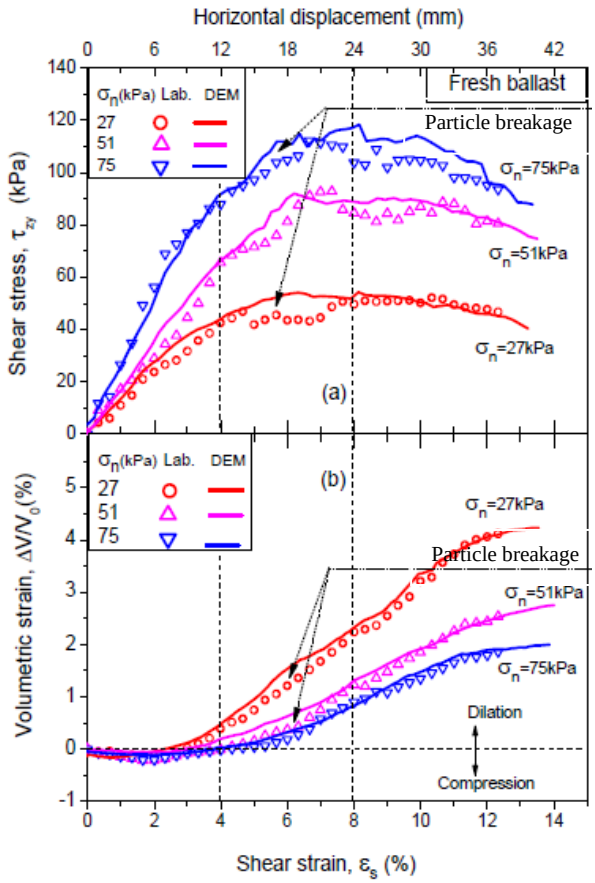


*Fig. 13. Comparisons between the DEM simulation and experiment for fresh ballast at 3 normal stresses of 27kPa, 51kPa, and 75kPa, (a) shear stress versus shear strain, (b) volumetric strain versus shear strain (Indraratna et al. 2012b)*

The DEM analysis shows a noticeable discrepancy in stress-strain curves, i.e. markedly decreased stress and retarded dilation shown by the experimental data at a shear strain of 4-8% compared to the predicted line. This difference may be attributed to some particle degradation that could not be accurately captured in the DEM simulation. Indeed, owing to the breakage of ballast aggregates, the reduction in shear strength would also be accompanied by a decrease in dilation

Distribution of Contact Forces in Fresh and Fouled Ballast.

Figure 14 shows the evolution of chains of contact force in fresh and fouled ballast at VCIs ranging from 0% to 70%, at a normal stress of 51kPa. While the number of contacts increases significantly with an increased VCI, the peak contact forces decreases with an increasing VCI.

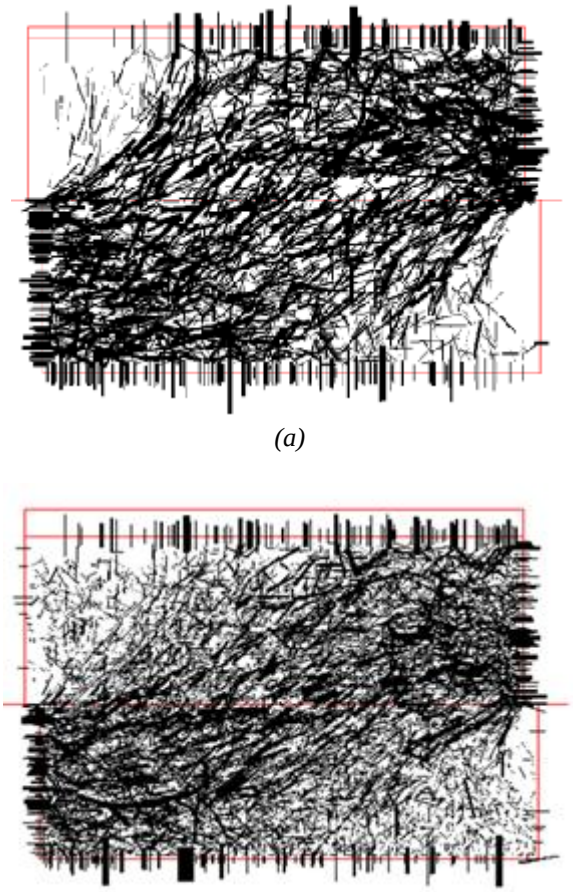

*(a)*

*(b)*

*Fig. 14. Evolution of the distribution of contact forces in fresh and fouled ballast at various VCIs (at 3% shear strain), (a) 0% VCI, (b) 20%VCI, (c) 40% VCI and (d) 70% VCI (Indraratna et al. 2012b)*

When there are coal fines in the voids, the applied load does not only transmit through the large aggregate skeleton but also across the fine coal particles. This results in a reduced maximum contact force magnitude corresponding to a higher number of particle contacts. Consequently, a more uniform distribution of stress is expected in the fouled ballast, as reflected by the distribution of a more dense contact force. The greater the VCI, the more prominent will be the corresponding uniform distribution of contact forces over a larger number of contacts, a result that may reduce ballast breakage by diminishing the intensity of stress concentrated in the fouled ballast matrix.

These micro-mechanical observations obtained from DEM clearly explain the reduced breakage of fouled ballast compared to fresh ballast as measured experimentally.

Influence of Train Speed

In this investigation the influence of train speed on the deformation and degradation of ballast during cyclic loading was studied using the large scale triaxial equipment as shown in Fig. 10 (Indraratna et al. 2010a). Latite ballast was thoroughly cleaned, dried, and compacted in four layers to a density of 1.53 tonnes/m$^3$. These specimens were then isotropically consolidated to a confining pressure of 60 kPa. Cyclic tests up to 100,000 load cycles were conducted at 10 Hz, 20 Hz, 30 Hz, and 40 Hz. Numerical model was developed in PFC$^{2D}$ to apply a stress controlled cyclic biaxial test at the desired frequency (f) and amplitude of cyclic loading. Sub-routines were developed to represent irregular ballast particles as shown in Figure 15.

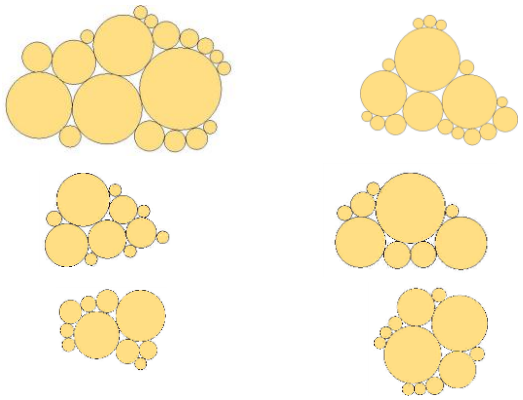

*Fig. 15. Representative ballast particles for DEM simulation*

Figure 16 presents the variation of axial strain ($\varepsilon_a$) with the number of cycles (N) for different frequencies (f) of loading. A significant increase in $\varepsilon_a$ with f was observed. For a particular value of f, $\varepsilon_a$ rapidly increased to maximum value (e.g, 6.1 % at N = 2,500 for f =10 Hz) in the initial cycles, after which a permanent $\varepsilon_a$ attained a stable value at large N. This sudden increase in $\varepsilon_a$ at low values of N could be attributed to the particle re-arrangement and corner breakage. In addition, it was evident that with an increase in f, higher values of N are required to stabilise $\varepsilon_a$.

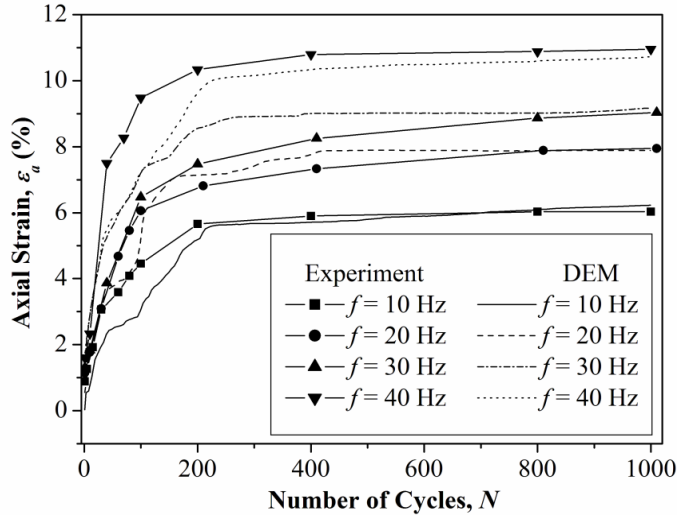


*Fig. 16. Comparison of axial strain ($\varepsilon_a$) predicted by DEM with experiment results (Indraratna et al. 2010a)*

The influence of frequency (f) and number of load cycles (N) on ballast breakage is presented in Fig. 17. Ballast breakage is measured using BBI for different values of f and N. The BBI is found to increase with f, but at lower values of f (e.g. f ≤30 Hz) BBI is not influenced by N. This clearly highlights that most ballast breakage takes place within 1000 cycles.

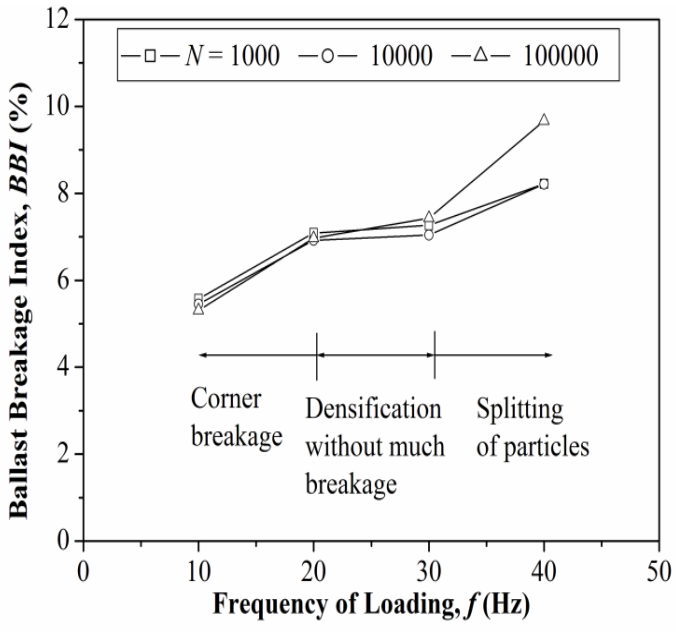


*Fig. 17. Variation of ballast breakage index (BBI) with various frequencies (f) (Indraratna et al. 2010a)*

A significant increase in BBI can be observed in the range 10 Hz ≤ f ≤ 20 Hz, a marginal increase in BBI in the zone 20 Hz < f ≤ 30 Hz, and a rapid increase in BBI as f > 30 Hz.

It has been observed from the laboratory tests that in the zone 10 Hz ≤ f ≤ 30 Hz, corner breakage is more pronounced, while considerable splitting of ballast particles can be observed at f > 30 Hz. In the range 20 Hz ≤ f ≤ 30 Hz, the ballast becomes denser under cyclic loading without much additional breakage. However, more pronounced breakage occurs as f > 30 Hz. High permanent deformation observed at higher frequencies can be attributed to an increase in particle degradation.

The cumulative bond breakage ($B_r$) is defined as a percentage of bonds broken compared to the total number of bonds. Figure 18 shows the variation of $B_r$ at different f and N. It is observed that $B_r$ increases with increase in f and N. Most of the bond breakages occurred during the initial cycles of loading, causing higher permanent $\varepsilon_a$. Once the bond breakage ceases, there is an insignificant increase in $\varepsilon_a$. This clearly highlights that particle degradation is one of the major sources responsible for permanent deformation.

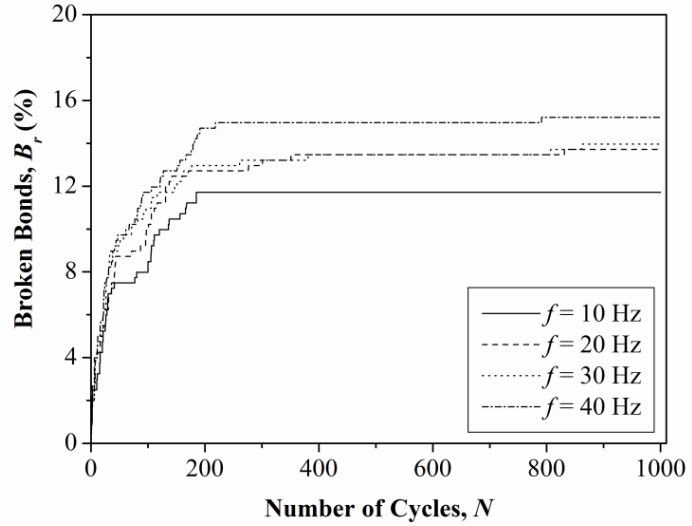


*Fig. 18. Effects of frequency (f) on bond breakage (Br) with number of cycles (N) (Indraratna et al. 2010a)*

## USE OF SHOCK MATS FOR MITIGATING BALLAST BREAKAGE INDUCED BY IMPACT

A series of laboratory tests were carried out to evaluate the effectiveness of shock mats in the attenuation of high frequency impact loads and subsequent mitigation of ballast deformations and degradation.

### Test Apparatus

Large scale drop-weight impact testing equipment was used for this study as shown in Fig. 19. The impact testing equipment consists of a free-fall hammer of 5.81 kN weight that can be dropped from a maximum height of 6 m with an equivalent maximum drop velocity of 10 m/s. To eliminate surrounding noise and ground motion, an isolated concrete foundation (5.0 m × 3.0 m × 2.5 m) was designed to bear a significantly higher fundamental frequency than the test apparatus.

### Material Specifications

The particle size distribution of ballast specimens was prepared in accordance with the current practice in Australia [AS 2758.7, 1996]. A thin layer of compacted sand was used in the laboratory physical model to simulate a typical ‘weak’ subgrade. The 10 mm thick shock mat used in the study was made of recycled rubber granulates of 1-3 mm size particles, bound by polyurethane elastomer compound (tensile strength = 600 kN/m$^2$, tensile strain at failure = 80%, Modulus at 10% compressive strain = 3800 kN/m$^2$).


*Fig. 19. Drop weight impact testing equipment.*

Test procedure

The ballast was thoroughly cleaned, dried, sieved through a set of standard sieves (aperture size 53: 13.2 mm). The ballast specimens ($C_u$ = 1.6, $C_c$ = 1.0, and $d_{50}$ = 35 mm) were compacted in several layers to simulate the field densities of heavy haul tracks. In order to resemble low track confining pressure in the field, test specimens were confined in a rubber membrane. A steel plate (t = 50 mm) was used to represent a hard base. In order to simulate relatively weak subgrade conditions, a 100 mm thick, vibro-compacted sand cushion was placed below the ballast bed. Three layers of shock mat accounting to a total thickness of 30 mm were used. The drop hammer was raised mechanically to the required height and then released by an electronic quick release system. The impact load was stopped after 10 blows due to an attenuation of strains in the ballast layer.

Results and discussion

Impact loading. Two distinct force peaks are generally observed during impact loading, an instantaneous sharp peak, $P_1$ with very high frequency and $P_2$, and a gradual peak of smaller magnitude with relatively lesser frequency (Jenkins *et al.* 1974). $P_2$ force showed a gradual increase with the increased number of blows as shown in Fig. 20. This was because the ballast develops a denser (compressed) packing assembly due to reorientation and rearrangement of ballast aggregates. A dense aggregate matrix offers a higher inertial resistance which leads to an increased value of $P_2$. A rapid increase of $P_2$ occurred at the initial stages of impact loading, but became almost insignificant after the eighth blow. This indicates that the ballast mass stabilises after a certain number of impacts to produce an almost constant $P_2$. Even without a shock mat, a ballast bed on a weak subgrade leads to a decreased magnitude of impact force compared to a stiffer subgrade.

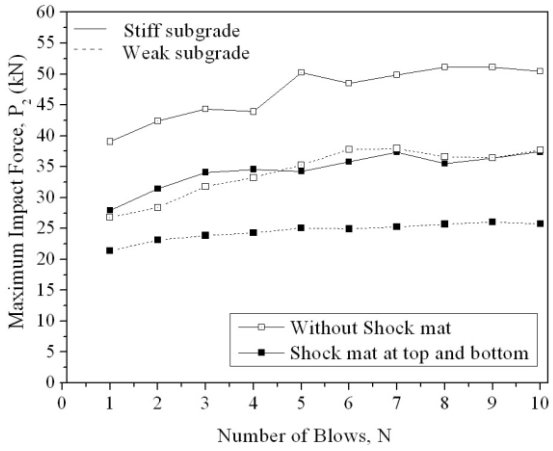


*Fig. 20. Variation of impact force with number of blows (data sourced from Nimbalkar et al. 2012).*

Ballast breakage. Particle degradation adversely affects the strength and deformation of ballast (Selig and Waters 1994, Indraratna *et al.* 2005, 2009, 2012c, Indraratna and Nimbalkar 2011). After each test, ballast sample was sieved to obtain BBI. The BBI values are presented in Table 3.

Table 3. Ballast breakage under impact loading (Indraratna *et al*. 2011b).

| Test No. | Base type | Shock Mat Details | *BBI* |
|---|---|---|---|
| 1 | Stiff | Without shock mat | 0.170 |
| 2 | Stiff | Shock mat at top and bottom | 0.091 |
| 3 | Weak | Without shock mat | 0.080 |
| 4 | Weak | Shock mat at top and bottom | 0.028 |

The higher breakage of ballast particles can be attributed to the considerable non-uniform stress concentrations occurring at the corners of the sharp angular particles. The application of just 10 impact blows caused considerable ballast breakage (i.e.

*BBI* = 17%) when a stiff subgrade was used but when a shock mat was placed above and below the ballast bed, particle breakage was reduced by approximately 47% for a stiff subgrade and about 65% for a relatively weak subgrade.

## USE OF GEOGRID FOR STABILISING BALLASTED TRACK: LABORATORY ASSESSMENT

In order to investigate the effect of the size of the geogrid aperture on the strength of the ballast-geogrid interface for different types of geogrids, a series of large scale direct shear tests were conducted. Fresh latite basalt with recommended gradations ($D_{50}$ = 35 mm) and seven geogrids with different aperture sizes (A) were used for this study. Their physical characteristics and technical specifications are given elsewhere (Indraratna *et al.* 2011b). A geogrid was placed at the interface of the upper and lower sections of the shear box assembly with the machine direction placed parallel to the direction of shearing. Tests were conducted at normal pressures of 26.3, 38.5, 52.5, and 61.0 kPa, using a shear rate of 2.75 mm/min. All tests were conducted to a maximum shear displacement of 36 mm. The behaviour of the ballast-geogrid interface could be examined on the basis of the interface efficiency factor ($\alpha$) which is defined as the ratio of the shear strength of the interface to the internal shear strength of the soil. Figure 21 shows the variation of $\alpha$ with $A/D_{50}$ ratio. It was observed that $\alpha$ increased with $A/D_{50}$ until it attained a maximum value of 1.16 at $A/D_{50}$ of 1.21, and then decreased towards unity as $A/D_{50}$ approached 2.5. The value of $\alpha < 1$ indicated that the particles were not interlocked, whereas when $\alpha > 1$ they were, which effectively increased the shear strength. Based on this variation of $\alpha$, the ratio $A/D_{50}$ was classified into three primary zones, as explained below:

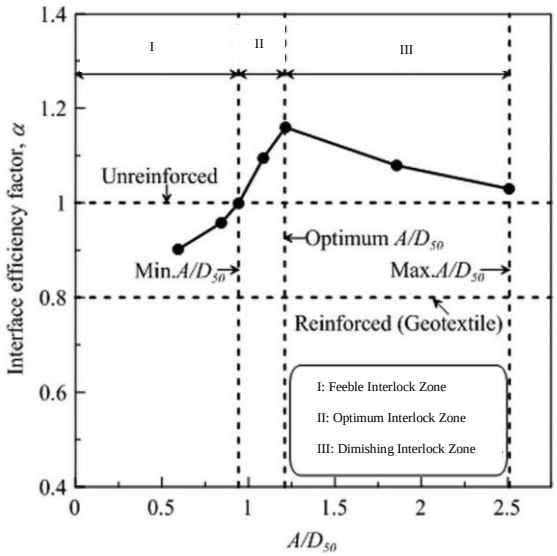


*Fig. 21. Variation of interface efficient factor ($\alpha$) with $A/D_{50}$ ratio (Indraratna et al., 2011b, Reprinted with permission from ASTM Geotechnical Testing Journal, copyright ASTM International, 100 Barr Harbor Drive, West Conshohocken, PA 19428)*

Feeble interlock zone ($0.95>A/D_{50}>0$)

In this zone the particle-grid interlock was weaker than the inter-particle interaction achieved without geogrid, because, the particle-grid interlock was only attributed to smaller particles ($<0.95D_{50}$) compared to the particle-particle interlock with respect to all sizes. An examination after testing showed insignificant particle breakage, which suggests the interface failure originated from a loss of particle-grid interlock during shearing.

Optimum interlock zone ($1.20>A/D_{50}>0.95$)

In this zone, the interlocking of relatively larger particles occurred, which contributed to values of $\alpha$ exceeding unity. The value of $\alpha$ attained a maximum of 1.16 at an optimum $A/D_{50}$ ratio of about 1.20. An examination after shearing showed there were many broken particles at the interface, suggesting that the failure was caused by the breakage of initially interlocked particles.

Diminishing interlock zone ($A/D_{50}>1.20$)

In this zone, the values of $\alpha$ were greater than unity but the degree of interlocking decreased rapidly, leading to a reduction in $\alpha$ with an increasing $A/D_{50}$ ratio. It was observed that $\alpha$ decreased to almost unity when $A/D_{50}$ exceeded 2.50. This implies that the interface responds in a similar manner as unreinforced ballast as the apertures increase in size in relation to the sizes of the ballast particles.

The minimum and maximum size apertures of geogrid required to achieve maximum efficiency was $0.95D_{50}$ and $2.50D_{50}$ respectively. For all practical purposes, the optimum size aperture of geogrid can be $1.15\text{-}1.3D_{50}$.

## FIELD STUDY: BULLI

In order to assess the stress-strain response of composite track substructure and the benefits of using geosynthetics in fresh and recycled ballast, a field trial was undertaken at Bulli in the State of New South Wales (NSW), Australia (Indraratna *et al.* 2010c).

Track Construction

The proposed site for track construction was located between two turnouts at Bulli, along the south coast of NSW. The instrumented section of track was divided into four 15 m long sections. The load bearing ballast and subballast were 300 mm and 150 mm thick, respectively. A layer of geocomposite was used below the fresh and recycled ballast (Fig. 22).

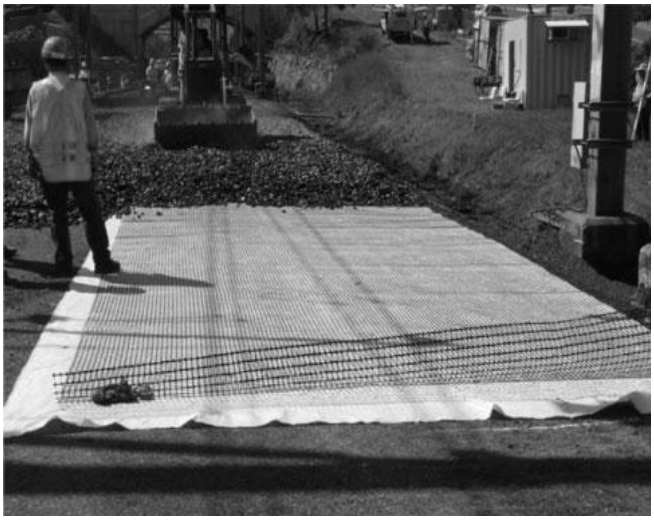

*Fig. 22. Installation of geocomposite under the ballast at Bulli.*

Material Specifications

The particle gradation of fresh ballast was in accordance with the Technical Specification TS 3402 (RailCorp, Sydney). Recycled ballast was collected from spoil stockpiles of Chullora yard near Sydney. The sub-ballast was a mixture of sand and gravel. The layer of geocomposite consisted of bi-axial geogrid and non-woven polypropylene geotextile. The particle size distributions of various materials and technical specifications of geosynthetics used during the track construction are given in Indraratna *et al*. (2010c).

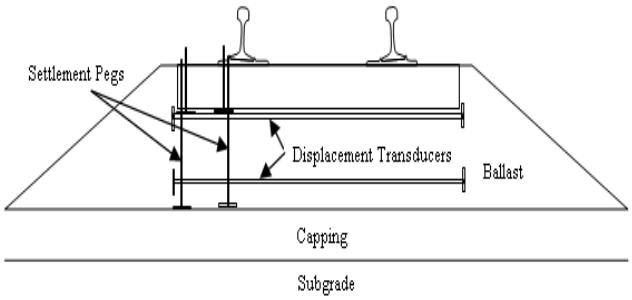


*Fig. 23. Installation of settlement pegs and displacement transducers in experimental sections of track at Bulli.*

Track Instrumentation

The performance of the experimental section was monitored using a series of sophisticated instruments. The vertical and horizontal stresses developed in the ballast were measured by earth pressure cells based on semi-conductor type transducers. Vertical and lateral deformations were measured by settlement pegs and electronic displacement transducers, respectively. These transducers were placed inside two, 2.5 m long stainless steel tubes that can slide over each other, with 100 mm × 100 mm end caps as anchors. The settlement pegs consisted of 100 mm × 100 mm × 6 mm stainless steel base plates attached to 10 mm diameter steel rods. The settlement pegs and displacement transducers were installed between the sleeper and ballast, and between the ballast and sub-ballast, respectively (Fig. 23).

Track Measurements

Vertical and horizontal deformations were measured in the field, against time. A relationship between the annual rail traffic in million gross tons (MGT) and axle load ($A_t$) was used to determine the number of load cycles (Selig and Waters, 1994):

$$C_m = \frac{10^6}{(A_t \times N_a)} \quad (7)$$

where $C_m$ = number of load cycles/MGT; $A_t$ = axle load in tons; and $N_a$ = number of axles/load cycle. Considering an annual tonnage of 60 MGT of traffic, and four axles per load cycle, an axle load of 25 tons gives 600,000 load cycles for 60 MGT per annum. Therefore, the results were plotted against the time and number of load cycles, as discussed below.

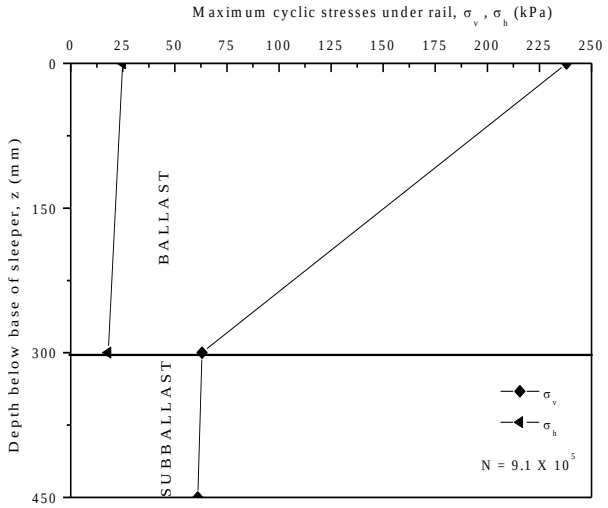


*Fig. 24. Vertical and horizontal maximum cyclic stresses (σv, σh) (data sourced from Indraratna et al. 2010c).*

Traffic induced peak stresses in ballast. Fig. 24 shows the vertical and horizontal maximum cyclic stresses ($\sigma_v$, $\sigma_h$) recorded in an unreinforced Section, under the rail and the edge of the sleeper, from a passenger train travelling at 60 km/h. The large vertical stresses and relatively small lateral (confining) stresses caused large shear strains in the track. The

corresponding ease of lateral spreading due to the absence of sufficient confinement increased the vertical compression of the ballast layer. Also, $\sigma_v$ and $\sigma_h$ increased with an increase in the number of load cycles, which further degraded the track bed.

Average lateral deformation. The average vertical and lateral deformations were determined from the mean of measurements between the sleeper and ballast, and between the ballast and sub-ballast. The average vertical and lateral deformations are plotted against the time scale (days) and number of load cycles (N) in Fig. 25. The recycled ballast showed improved performances, i.e. less vertical and lateral deformations, because of its moderately graded particle size distribution compared to the very uniform fresh ballast.

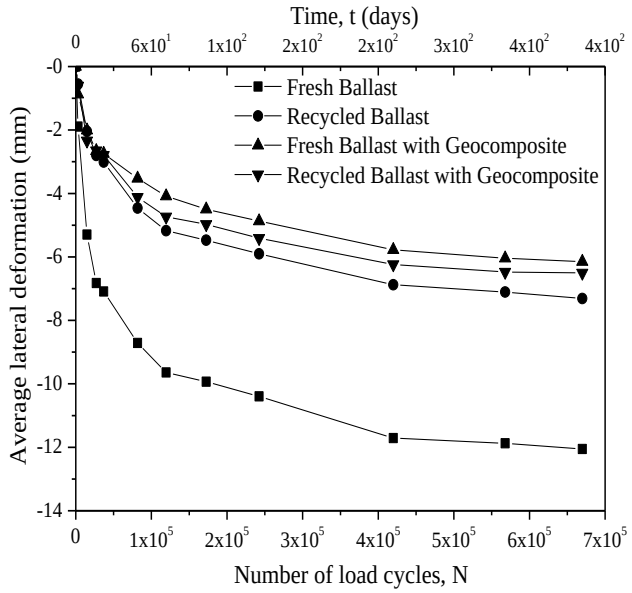


*Fig. 25. Average lateral deformations of the ballast (data sourced from Indraratna et al. 2010c).*

If a layer of ballast is placed with a moderately graded grain size distribution, the corners of individual particles may not break so frequently because of their reduced angularity. The geocomposite reduced the lateral deformation of fresh ballast by about 49% and recycled ballast by 11%. The apertures of the geocomposite offered a strong mechanical interlock with the ballast, forming a highly frictional interface.

## FIELD STUDY: SINGLETON

### Track Construction

Construction of the track was started in July 2009 and the track was commissioned in May 2010. An extensive program of sub-surface exploration, consisting of 33 bore holes and 107 test pits, indicated that the Third Track was located on a massive sedimentary outcrop of rock, between 224.20 to 229.00 km, and later on the flood plain of the nearby Hunter River (RCA Australia 2008).

The rock outcrop was part of the Branxton Formation and mainly composed of medium to high strength siltstone. The flood plain consisted of a layer of an alluvial deposit of silty clay 7-10 m thick, underlain by heterogeneous layers of medium dense sand and silty clay with a total thickness of 7-9 m. Medium strength siltstone, similar to the first part of track, was found beneath the layer of sand and silty clay.

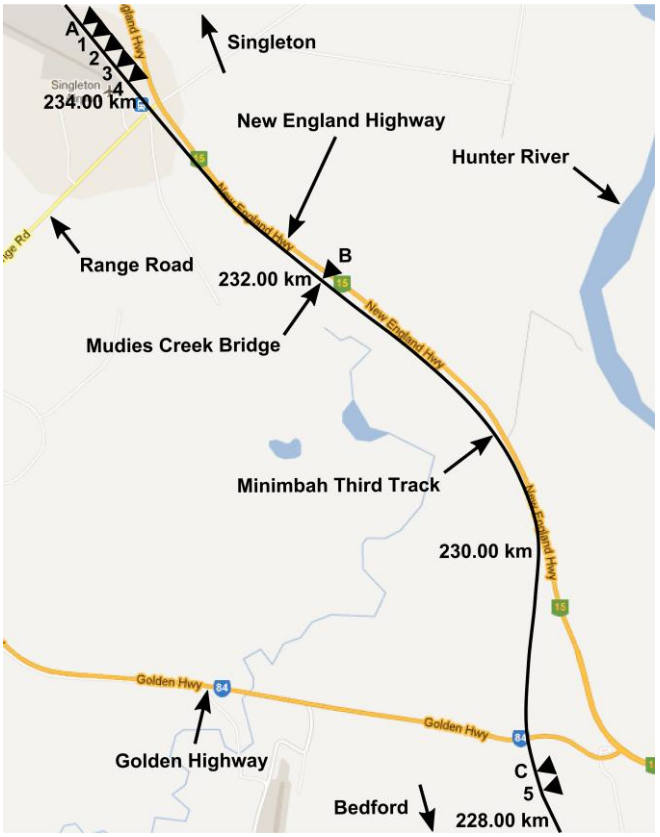


*Fig. 26. Locations of Minimbah Third Track sections with different values of subgrade stiffness.*

To investigate how well different types of geosynthetics would improve the overall stability of the track under in situ conditions, an extensive study was undertaken on fully instrumented sections of track.

Nine experimental sections were included in the Third Track while it was under construction, on three different types of sub-grades, including (i) the relatively soft general fill and alluvial silty clay deposit (Sections 1-5 and Section A), (ii) the intermediate cut siltstone (Sections 6 and C), and (iii) the stiff reinforced concrete bridge deck supported by a piled abutment (Section B), as shown in Fig. 26 and Table 4.

Table 4. Reinforcement at experimental sections using geogrids, geocompolistes, and shock mats.

| Section | Location | Reinforcement |
|---|---|---|
| A | 234.75 | - |
| 1 | 234.66 | Geogrid 1 |
| 2 | 234.40 | Geogrid 2 |
| 3 | 234.22 | Geogrid 3 |
| 4 | 234.12 | Geocomposite |
| B | 232.01 | Shock mat |
| C | 228.50 | - |
| 5 | 228.44 | Geogrid 3 |

Material Specifications

The substructure of the track consisted of a 300 mm thick layer of ballast ($D_{50}$ = 36 mm, angular latite basalt fragments) underlain by a 150 mm thick layer of sub-ballast (GP-GM, compacted sandy gravel, CBR $\geq$ 50%, $d_{50}$ = 4 mm). A structural layer of fill with a minimum of 500 mm thickness (GP-GM, compacted sandy gravel, CBR $\geq$ 30%, $d_{50}$ = 3 mm) was placed below the sub-ballast. The gradation and classification (at the time of commission) of the materials used to construct these components are shown in Fig. 27.

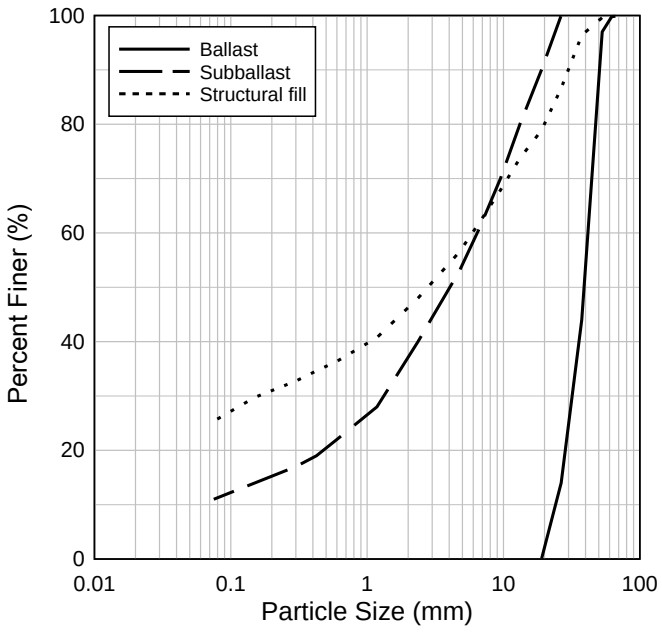


*Fig. 27. Particle size distribution of materials used during track construction*

Although these materials had different particle gradations, they were all obtained from the same quarry (20 km northwest of Singleton) and were composed of similar minerals. Three commercially available geogrids, namely EnkaGrid, TensarGrid, TerraGrid, and one geocomposite i.e. CombiGrid (geocomposite) were installed in a single layer at the ballast-sub-ballast interface to investigate the key influential factors, i.e., the stiffness, aperture size, and filtration ability under 'field' conditions. The properties of the geosynthetics used in this study are listed in Table 5. The properties reported in the table are in the 'machine' direction followed by those in the 'cross-machine' direction. For comparison purposes, no geosynthetic was installed at Sections A and C. A layer of shock mat was installed between the ballast and bridge deck at Section B to minimise any degradation of the ballast. The relevant properties of the shock mat are listed in Table 6.

Table 5. Mechanical properties of geogrids and geo composites (* indicates values in "machine'" direction followed by "cross-machine" direction).

| | Geogrid 1 | Geogrid 2 | Geogrid 3 | Geocomposite | |
|---|---|---|---|---|---|
| Material | polypropylene | | | Polypropylene | |
| Type | biaxial | | | (grid) biaxial | (fabric) nonwoven |
| Tensile stiffness* (MN/m) | 1.8/1.8 | 1.5/1.5 | 1.5/1.5 | 2.0/2.0 | 0.3/0.5 |
| Tensile strength* (kN/m) | 36/36 | 30/30 | 30/30 | 40/40 | 6/10 |
| Strain at break (%) | 15/15 | 15/15 | 15/15 | 15/15 | 60/40 |
| Aperture size* (mm) | 44/44 | 65/65 | 40/40 | 31/31 | - |
| Thickness (mm) | 3 | 3 | 4 | 3 | 2.9 |

Table 6. Mechanical properties of shock mats.

| Material | Polyurethane elastomer |
|---|---|
| Type | Bonded rubber granulates |
| Particle size (mm) | 1-3 |
| Tensile strength (kN/m$^2$) | 600 |
| Strain at break (%) | 80 |
| Thickness (mm) | 10 |

Track Instrumentation

Figure 28 shows how the instruments were installed at the experimental sections of track to study its behavior under repetitive traffic loads. Strain gauges were used to study deformations and mobilised forces along the layers of geogrid (Fig. 28a). Traffic induced vertical stresses were monitored by pressure cells. Transient deformations of the ballast were measured by five potentiometers (POTs) mounted on a custom built aluminum frame, as shown in Fig. 28c. Settlement pegs were installed between the sleeper and ballast and between the ballast and sub-ballast to measure vertical deformations of the ballast (Fig. 28d). The strain gauges were a post yield type suitable to measure tensile strains between 0.1 to 15%. They were installed in a group, about 200 mm apart, on the top and

bottom sides of the grids, in both the longitudinal and transverse directions (Fig. 28a). At each section, one group of strain gauges was installed below the edge of the sleeper, while another was below the up rail. Protective layers made of vulcanized rubber were used to cover the strain gauges to minimise any damage caused by contact with the ballast. Flexible aluminum sleeves were also used to protect the data cables of the strain gauges, as shown in Fig. 29.

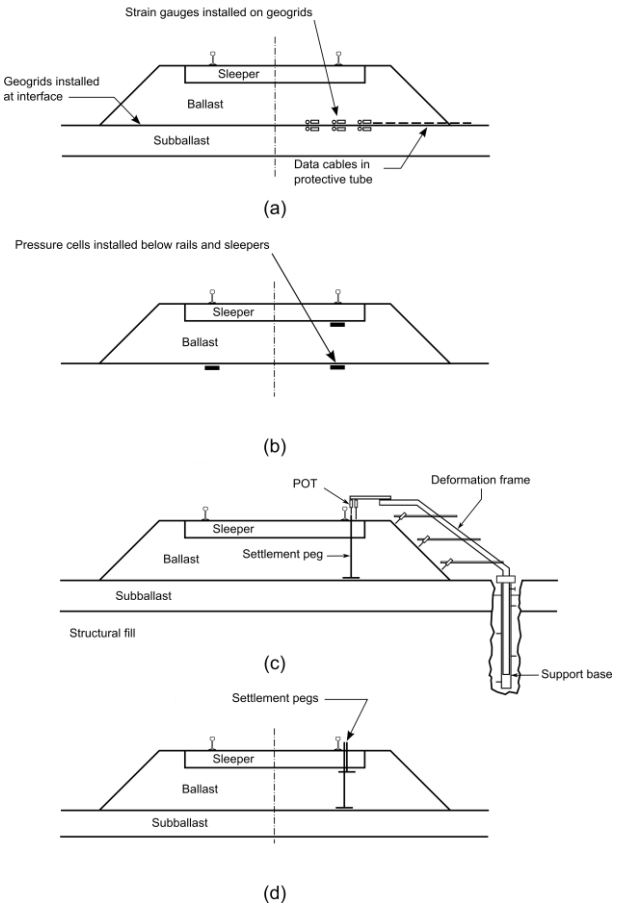


*Fig. 28. Details of instrumentation of experimental sections of track at Singleton using, (a) strain gauges, (b) pressure cells, (c) deformation frame and (d) settlement pegs.*

Two pressure cells were installed at Sections 1, 6, A, and C, one directly below the ties and the other directly above the layer of sub-ballast (Fig. 28b). To install them, the ballast was removed and the sub-ballast was levelled. The cells were then placed in position and the ballast backfilled, as shown in Fig. 30. At Section B, three pressure cells were installed between the synthetic mat and the deck. Two cells were located below the up rail, while the other was below the down rail. The two POTs were mounted vertically on the frame (Fig. 28c), one to monitor movement of the sleepers, and the other to measure the movement of settlement peg placed at top of the sub-ballast. The other three POTs were mounted in an inclined fashion to monitor the vertical and horizontal deformations of the shoulder of the ballast at different locations. The deformation frame was held in place by support bases installed in the sub-ballast and layers of structural fill.

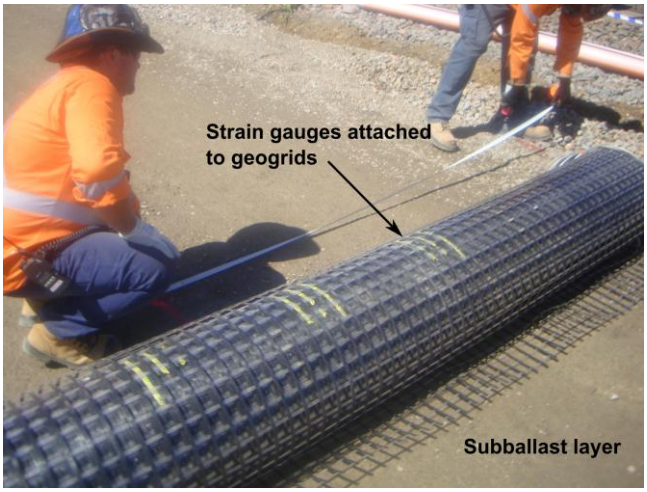


*Fig. 29. Strain gauges are covered with several layers of protective coats. Data cables are routed in protective aluminum sleeves to avoid cuts from ballast particles.*

Electrical analogue signals from the strain gauges, pressure cells, and potentiometers were obtained using a mobile data acquisition (*DAQ*) unit shown in Fig. 31. The unit consisted of a National Instrument model 9188 module working in parallel with a mobile personal computer.


*Fig. 30. Installation of pressure cells involves removing and backfilling the ballast.*

The data acquisition module and associated wiring was housed in a custom made, aluminum case. The module provided electrical excitations and received signals from the instruments. The input signals were amplified and filtered to reduce signal noises. These 'conditioned' signals were

converted into a digital format and then later in real time in the mobile computer. The data acquisition module was configured and controlled by a computer program written in the National Instrument's LabView environment.

All the field measurement were obtained from the aforementioned instruments at a frequency of 2000 Hz. A 12V automotive battery provided a direct current power supply to the data acquisition module. Alternating power for the mobile computer was also provided by the same battery, but via an inverter.

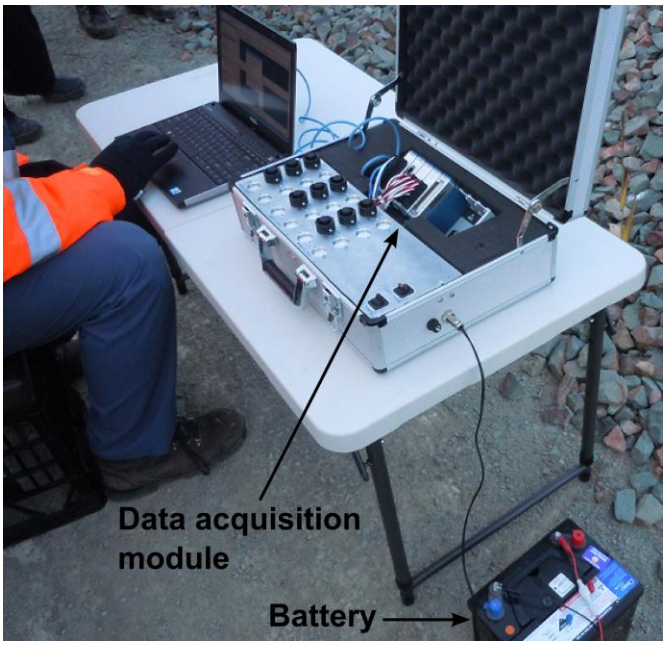


*Fig. 31. DAQ module connected to laptop.*

Track Measurements

Long-term Settlement of Ballast. The settlement ($S_v$) and vertical strain ($\varepsilon_v$) of the ballast after about 100,000 load cycles, or 40 days after the track was commissioned, and about 300,000 load cycles or 120 days, are reported in Table 7. These preliminary results indicate that the relationship between the settlement of ballast and the number of load cycles (N) is non-linear, regardless of how the track was reinforced. The rate at which settlements increased, decreased as the number of load cycles increased.

Table 7. Vertical settlement and strain of the ballast layer after (a) 100,000 load cycles and (b) 300,000 load cycles.

| Section | A | 1 | 2 | 3 | 4 | B | C | 5 |
|---|---|---|---|---|---|---|---|---|
| $\varepsilon_v$ (%) (N= 50,000) | 5.1 | 4.0 | 4.3 | 2.4 | 3.9 | 1.0 | 3.0 | 2.7 |
| $\varepsilon_v$ (%) (N=100,000) | 7.0 | 5.4 | 6.1 | 3.9 | 5.1 | 2.0 | 5.1 | 4.2 |

When the results for sections on similar subgrades were compared to each other, vertical settlements of the reinforced sections were 10-32% smaller than those without reinforcement. This pattern is similar to that observed in the laboratory (Shin et al. 2002 and Brown et al. 2007), and is mainly attributed to the interlocking between ballast particles and grids, as discussed earlier. When the results for sections with similar geogrids are compared, it is apparent that the ability of geogrid reinforcement to reduce track settlement is generally higher for softer subgrades (low track stiffness). Such an observation is in agreement with the results of the full scale laboratory tests presented by Ashmawy and Bourdeau (1995).

Moreover, of the four types of synthetics used, TerraGrid performed most effectively. Although the stiffness of TerraGrid is equal to or lower than the others, its aperture size (40 mm) enabled better interlocking between the ballast particles and grids. This finding also agrees with the criteria for optimum size apertures for reinforcing geogrids proposed by Brown *et al.* (2007). When Sections A, B, and C are compared, the results indicate that the vertical settlements are larger when the subgrade becomes weaker (low track stiffness), i.e., vertical settlement was smaller at the section on the concrete bridge deck (B) and larger than the section on the alluvial deposit (A).

Transient Deformations of Ballast. Transient deformations of the ballast layer were measured by the deformation frame. It was observed that the passage of trains with an axial load of 30 tons travelling at 40 km/h resulted in a vertical deformation ($S_{tv}$) between 1.5 to 3.0 mm, resulting in average vertical strain ($\varepsilon_{tv}$) of between 0.5 and 1.0%. The transient horizontal deformations of ballast ($S_{th}$) measured on the shoulder (up rail side) were all expansive and between -0.5 to -0.3 mm. This resulted in an average horizontal strain ($\varepsilon_{th}$) of -0.05 to -0.02%. The horizontal strains were larger near the crest and smaller near the toe of ballast. The average transient strains of track sections with reinforcement were about 15% smaller than those without reinforcement, regardless of the type of geosynthetics used.

Traffic Induced Vertical Stresses. The vertical stresses ($\sigma_v$) due to the passage of trains with an axle load of 30 tons travelling at about 40 km/h were about 280 kPa at Section B (mat-deck interface) and between 30 to 40 kPa at Sections 1, 6, A, and C (ballast-sub-ballast interface). Vertical stresses at the sleeper-ballast interface of the latter sections were between 170 to 190 kPa, which indicate that the traffic-induced stresses were considerably larger in the track with a stiffer subgrade.

The larger stresses also caused much more breakage of individual particles of ballast, as was anticipated. The ballast breakage index (BBI) after 750,000 load cycles (300 days after the track was commissioned) for Sections B was 17%, while Sections A and C were 9.8% and 13.1%, respectively. This finding appears to contradict the general perception that ballast subjected to higher stresses (Section B) would undergo

larger settlements and vertical strains due to larger degrees of particle breakage (Lackenby *et al*. 2007, Nimbalkar *et al*. 2012). This is because the ballast at Section B was contained within the barriers of the Mudies Creek bridge, which meant that the ballast could not spread laterally. At Sections A and C however, ballast was allowed to expand more freely in a horizontal direction, and larger vertical settlement was thus observed. This observation also confirms that the ability of ballast to expand horizontally also influences the magnitude of track settlement as well as the degree of ballast breakage.

Table 8. Typical values of accumulated longitudinal and transverse strains in geogrids after (a) 100,000 cycles and (b) 300,000 load cycles.

| Section | 1 | 2 | 3 | 4 | 5 |
|---|---|---|---|---|---|
| $\varepsilon_l$ (%) (N=50,000) | 0.75 | 1.00 | 0.55 | 0.38 | - |
| $\varepsilon_t$ (%) (N=50,000) | 0.75 | 0.74 | 0.76 | 1.35 | 0.65 |

(a)

| Section | 1 | 2 | 3 | 4 | 5 |
|---|---|---|---|---|---|
| $\varepsilon_l$ (%) (N=100,000) | 0.78 | 1.04 | 0.61 | 0.42 | - |
| $\varepsilon_t$ (%) (N=100,000) | 0.79 | 0.72 | 0.78 | 1.40 | 0.68 |

(b)

Strains in Geosynthetics. Accumulated longitudinal ($\varepsilon_l$) and transverse ($\varepsilon_t$) strains after 100,000 and 300,000 load cycles, as measured by the bottom strain gauges installed below the edges of sleepers, are given in Table 8. Here, most of permanent strains in the geogrids in both directions developed when the track was being constructed, particularly when the ballast was being placed. In general, the strains did not change very much with the number of load cycles. As shown in Table 8, the transverse strains were generally larger than the longitudinal strains, probably due to confinement or a higher level of longitudinal restraint relative to the transverse direction.

The values of $\varepsilon_l$ and $\varepsilon_t$ also appear to be mainly influenced by deformation of the subgrade. The transverse strains developed in the CombiGrid (Section 5) were relatively large, although being stiffer they could have been expected to result in smaller strains because the embankment was constructed from alluvial silty clay and siltstone cuttings, and at this location underwent large lateral deformation shortly after the track was commissioned, which resulted in excessive transverse strains in the geocomposite.

Induced transient strains in both the longitudinal ($\Delta\varepsilon_{lt}$) and transverse ($\Delta\varepsilon_{tt}$) directions due to the passage of trains with an axial load of 30 tons travelling at 40 km/h were between 0.14-0.17%. Unlike the accumulated strains, the values of $\Delta\varepsilon_{lt}$ and $\Delta\varepsilon_{tt}$ were smaller in grids with higher values of stiffness, but the transient strains in the geogrids were very consistent, and therefore were independent of the number of load cycles.

## CONCLUSIONS

This SOAP paper discusses results of large-scale laboratory tests, numerical modeling using finite element method and discrete element method as well as the findings from full-scale instrumented track.

The detrimental effects of fouling on the strength and drainage characteristics were assessed using a new parameter, the Void Contaminant Index (VCI). A series of isotropically consolidated drained monotonic triaxial tests using a large scale cylindrical triaxial apparatus were conducted on clay fouled ballast. Based on the laboratory findings, a novel empirical relationship between the peak deviator stress and VCI was proposed with the aim of assisting the practitioner in the preliminary track assessment.

The large scale direct shear tests revealed that inclusion of coals into ballast layer reduced the shear strength of ballast. The DEM model captured the shear stress-strain response and volumetric changes observed in the laboratory experiments. The laboratory studies show that permanent deformation and degradation increased with the frequency and number of cycles, but in a 20 Hz $\leq$ f $\leq$ 30 Hz zone, cyclic densification was observed without significant additional ballast breakage. The DEM based micro-mechanical investigation showed that most particles break during the initial cycles, which leads to higher initial axial strains.

The large-scale laboratory test results revealed that the shock mats could decrease impact induced strains in ballast by as much as 50%. Impact caused the most significant damage to ballast, especially under high repetitive loads, while just few impact blows caused considerable ballast damage (i.e. BBI = 17%) when a stiff subgrade was used. However, when a shock mat was placed at the top and bottom of the ballast bed, particle breakage was reduced by approximately 47% over a stiff subgrade. It was also observed that the normalised aperture ratio, ($A/D_{50}$) had a profound influence on the interface efficiency factor ($\alpha$). The best size geogrid aperture to optimise the interface shear strength was $1.20D_{50}$. The minimum and maximum sized apertures required to attain the beneficial effects of geogrids were $0.95D_{50}$ and $2.50D_{50}$, respectively.

The results of the Bulli case study indicated that the use of geocomposite as reinforcing elements for recycled ballasted tracks proved to be a feasible and effective alternative. The test results demonstrated the potential benefits of using a geocomposite in track, where it was able to reduce the lateral deformation of fresh ballast by about 49% and recycled ballast by 11%. The preliminary results of the Singleton study

showed that geogrids could decrease the vertical strains of the ballast, with the obvious benefits of reducing the rate of deterioration of track geometry and decreasing the cost of maintenance. The effectiveness of this reinforcement increased as the subgrade decreased in stiffness. Transient strains of the ballast layer also decreased when geosynthetics were used. The strains that accumulated in the geogrids were influenced by the placement of the ballast and deformation of the subgrade, while the induced transient strains were mainly affected by the stiffness of the geogrids. The findings of these field studies allows for a better assessment of the ability of geosynthetic reinforcement to mitigate degradation caused by cyclic and impact wheel loads, as well as more economical and effective design and maintenance of ballasted rail tracks.

## ACKNOWLEDGEMENTS

The authors are grateful to the CRC for Rail Innovation (established and supported under the Australian Government's Cooperative Research Centres program R3.106 &R3.117) for the funding of this research. The authors express their sincere thanks to Australian Research Council, RailCorp (Sydney), ARTC and Queensland Rail National for their continuous support. The Authors would like to thank Dr Pongpipat Anantanasakul (Lecturer, Mahidol University, Thailand) for his help during the preparation of this manuscript. A number of current and past PhD students, namely Miss Nayoma Tennakoon, Mr Sd K Karimullah Hussaini, Mr Ngoc Trung Ngo, Dr Joanne Lackenby, Dr Daniela Ionescu, Dr Wadud Salim and Dr Pramod Kumar Thakur have participated to the contents of this paper and their contributions are greatly acknowledged. The Authors would also like to thank Dr Jayan Vinod (University of Wollongong, Wollongong). The assistance of Mr David Christie (formerly Senior Geotechnical Consultant, RailCorp), Mr Tim Neville (ARTC), Mr Michael Martin (QR National) and Mr Sandy Pfeiffer (RailCorp) is gratefully acknowledged. The authors would like to thank Mr. Alan Grant, Cameron Neilson and Ian Bridge (technical staff, University of Wollongong) for their assistance throughout the period of this study. The on-site assistance provided by Mr. David Williams of ARTC is also appreciated. A significant portion of the contents have been reproduced with kind permission from the Journal of Geotechnical and Geoenvironmental Engineering ASCE, International Journal of Geomechanics, ASCE, ASTM Geotechnical Testing Journal, Geotechnique, and Canadian Geotechnical Journal.

## REFERENCES

ARTC [2006]. "*Track Drainage–Design and Construction*" Engineering Practices Manual Civil Engineering, Australian Rail Track Corporation, Issue A, NSW, Australia.

Ashmawy, A.K. and P.L. Bourdeau [1995]. "Geosynthetic-reinforced soils under repeated loading: a review and comparative design study." Geosynthetics International, Vol. 2, No. 4, pp. 643-678.

ASTM Standard [2002]. "*Standard test method for consolidated undrained triaxial compression test for cohesive soils*", West Conshohocken, PA, ASTM International 2002, ASTM D4767-02.

Auersch, L. [2006]. "Dynamic axle loads on tracks with and without ballast mats: numerical results of three-dimensional vehicle-track-soil models", *Proceedings of the Institution of Mechanical Engineers*, Part F: Journal of Rail and Rapid Transit, Vol. 220, pp. 169-183.

Bishop A.W. and D.J. Henkel [1962]. "*The measurement of soil properties in the triaxial test*". Arnold, London.

Brown, S.F., J. Kwan and N.H. Thom [2007]. "Identifying the key parameters that influence geogrid reinforcement of railway ballast." Geotextiles and Geomembranes, Vol. 25, No. 6, pp. 326-335.

Charles J.A. and K.S. Watts [1980]. "The influence of confining pressure on the shear strength of compacted rockfill." Géotechnique, London, U.K., Vol. 30, No. 4, pp. 353-367.

Chrismer, S.M. [1985]. "Considerations of factors affecting ballast performance", Report No.WP-110, Administration of American Railroads, Research and Test Department, Bulletin 704, American Railway Engineering Association, pp. 118-150.

Feldman, F. and D. Nissen [2002]. "Alternative Testing Method for the Measurement of Ballast Fouling: Percentage Void Contamination", Conference on Railway Engineering, RTSA, Wollongong, pp. 101-109.

GeoStudio [2007]. "*SEEP/W for Finite Element Seepage Analysis*", Users Manual, Geo-Slope International, Calgary, Alberta, Canada.

Hirschfeld, R.C. [1973]. "*Embankment-Dam Engineering*", John John Wiley & Sons, New York.

Hossain, Z., B. Indraratna, F. Darve, and P. Thakur [2007]. "DEM analysis of angular ballast breakage under cyclic loading." Geomechanics and Geoengineering, Vol. 2, No. 3, pp. 175-181.

Indraratna B., D. Ionescu and D. Christie [1998]. "Shear behaviour of railway ballast based on large-scale triaxial tests", J. Geotech. Geoenviron. Eng., ASCE, Vol. 124, No. 5, pp. 439-439.

Indraratna B., S. Nimbalkar and D. Christie [2009], "The Performance of Rail Track Incorporating the Effects of Ballast Breakage, Confining Pressure and Geosynthetic Reinforcement", *Proceedings of 8th International Conference on the Bearing Capacity of Roads*, Railways, and Airfields, London: Taylor and Francis Group, pp. 5-24.

Indraratna, B. and S. Nimbalkar [2011]. "Implications of Ballast Breakage on Ballasted Railway Track based on Numerical Modelling", *Proceedings of 13th International Conference of International Association for Computer Methods and Advances in Computational Mechanics*, IACMAG 2011, Australia. pp. 1085-1092.

Indraratna, B. and S. Nimbalkar [2012] "Stress-strain-degradation response of railway ballast stabilised with geosynthetics", J. Geotech. Geoenviron. Eng. ASCE (accepted, in press).

Indraratna, B. and W. Salim [2003]. "Deformation and

degradation mechanics of recycled ballast stabilised with geosynthetics" Soils Found., Vol. 43, No. 4, pp. 35-46.
Indraratna, B., H. Khabbaz, W. Salim and D. Christie [2006]. "Geotechnical properties of ballast and the role of geosynthetics in rail track stabilization", Ground Improvement, Vol. 10, No. 3, pp. 91-101.
Indraratna, B., J. Lackenby and D. Christie [2005]. "Effect of confining pressure on the degradation of ballast under cyclic loading." Géotechnique, UK, Vol. 55, No. 4, pp. 325-328.
Indraratna, B., M.A. Shahin and W. Salim [2007]. "Stabilising granular media and formation soil using geosynthetics with special reference to Railway engineering", Ground Improvement, Vol. 11, No. 1, pp. 27-44.
Indraratna, B., N. Tennakoon, S. Nimbalkar and C. Rujikiatkamjorn [2012a]. "Behaviour of Clay Fouled Ballast under Drained Triaxial Testing", Géotechnique, 62(10) (in press).
Indraratna, B., N.T. Ngo, C. Rujikiatkamjorn and J.S. Vinod [2012b]. "Behaviour of fresh and fouled railway ballast subjected to direct shear testing - A discrete element simulation", Int. J. of Geomech. ASCE (accepted, in press).
Indraratna, B., N.T. Ngo and C. Rujikiatkamjorn [2011a]. "Behavior of geogrid-reinforced ballast under various levels of fouling", Geotextiles & Geomembranes, Vol. 29, pp. 311-322.
Indraratna, B., P.K. Thakur and J.S. Vinod [2010a]. "Experimental and Numerical Study of Railway Ballast Behavior under Cyclic Loading." Int. J. of Geomech. ASCE, Vol. 10, No. 4, pp. 136-144.
Indraratna, B., S. Nimbalkar and C. Rujikiatkamjorn [2012c]. "Track Stabilisation with Geosynthetics and Geodrains, and Performance Verification through Field Monitoring and Numerical Modelling", Int. J. of Railway Technology Vol. 1, No. 1, pp. 195-219.
Indraratna, B., S. Nimbalkar and N. Tennakoon [2010b]. "The behaviour of ballasted track foundations: track drainage and geosynthetic reinforcement", *GeoFlorida 2010*, ASCE Annual GI Conference, Florida, USA, pp. 2378-2387.
Indraratna, B., S. Nimbalkar, D. Christie, C. Rujikiatkamjorn and J.S. Vinod [2010c]. "Field assessment of the performance of a ballasted rail track with and without geosynthetics." J. Geotech. Geoenviron. Eng. Vol. 136, No. 7, pp. 907-917.
Indraratna, B., S.K. Hussaini and J.S. Vinod [2011b]. "On the shear behaviour of ballast-geosynthetic interfaces", Geotechnical Testing Journal, ASTM Vol. 35, No. 2, pp. 1-8.
Indraratna, B., W. Salim and C. Rujikiatkamjorn [2011c]. "*Advanced Rail Geotechnology - Ballasted Track*", CRC Press/Balkema.
Indraratna, B., L.S.S. Wijewardena and A.S. Balasubramaniam [1993]. Large-scale triaxial testing of greywacke rockfill. Géotechnique, Vol. 43, No. 1, pp. 37-51.
Jeffs, T. and G.P. Tew [1991]. "A Review of Track Design Procedures - Sleepers and Ballast", Vol. 2, Railways of Australia, Melbourne, 205p.
Jenkins, H.M., J.E. Stephenson, G.A. Clayton, J.W. Morland and D. Lyon [1974]. "The effect of track and vehicle parameters on wheel/rail vertical dynamic forces." Railway Engineering Journal, Vol. 3, pp. 2-16.
Lackenby, J., B. Indraratna, G. McDowell and D. Christie [2007]. "Effect of confining pressure on ballast degradation and deformation under cyclic triaxial loading." Géotechnique, Vol. 57, No. 6, pp. 527-536.
Marachi N.D., C.K. Chan and H.B. Seed [1972] "Evaluation of properties of rockfill materials". Journal of the Soil Mechanics and Foundations Division, ASCE, Vol. 96, No. 6, pp. 95-114.
Marsal, R.J. [1973]. "Mechanical properties of rock fill". In: Hirschfield R. C. and Pools, S. J. (eds) *Embankment Dam Engineering: Casagrande Volume*, Wiley, New York, pp. 109-200.
Nimbalkar, S., B. Indraratna, S.K. Dash, and D. Christie [2012]. "Improved performance of railway ballast under impact loads using shock mats." J. Geotech. Geoenviron. Eng., ASCE, Vol. 138, No. 3, pp. 281-294.
Pilgrim, D. H., 1997, Australian Rainfall and Runoff: A Guide to Flood Estimation, Institution of Engineers, Barton, ACT, Australia, pp. 15-54.
Raymond, G.P. [1979]. Railroad Ballast Prescription: State-of-the-Art. Journal of the Geotechnical Engineering Division, ASCE, Vol. 105, No. GT2, pp. 305-322.
Raymond, G.P. [2002]. "Reinforced ballast behaviour subjected to repeated load." Geotext. Geomembr. Vol. 20, No. 1, pp. 39-61.
RCA Australia [2008]. *Geotechnical Investigation Report for Minimbah Bank Third Track*. RCA Australia, Newcastle, Australia.
Selig, E.T. and J.M. Waters [1994]. "*Track Geotechnology and Substructure Management*", Thomas Telford, London. Reprint 2007.
Shin E.C., D.H. Kim and B.M. Das [2002]. "Geogrid-reinforced railroad bed settlement due to cyclic load." Geotechnical and Geological Engineering, Vol. 20, No. 3, pp. 261-271.
Standards Australia. [1996]. *Aggregates and rock for engineering purposes*, Part 7: Railway ballast AS 2758.7-1996. Sydney, NSW, Australia.
Standards Australia. [1999]. *Soil Strength and Consolidation Tests-Determination of Permeability of a Soil-Constant Head Method Using a Flexible Wall Permeameter*, Methods of Testing Soils for Engineering Purposes AS 1289.6.7.3. Sydney, Australia.
T. S. 3402 [2001]. *Specification for Supply of Aggregates for Ballast*. Rail Infrastructure Corporation of NSW, Sydney, Australia.
Tennakoon, N., B. Indraratna, C. Rujikiatkamjorn, S. Nimbalkar and T. Neville [2012]. "The role of ballast fouling characteristics on the drainage capacity of rail substructure", ASTM Geotech. Testing Journal, Vol. 35, No. 4, pp. 1-12.
Terzaghi, K. and P.B. Peck [1967]. "*Soil Mechanics in Engineering Practice*", John Wiley & Sons, New York.